On the filamentary environment of galaxies

C. Gay, C. Pichon, D. Le Borgne, R. Teyssier, T. Sousbie, J. Devriendt

Monthly Notices
of the
ROYAL ASTRONOMICAL SOCIETY

Mon. Not. R. Astron. Soc. **404,** 1801–1816 (2010) doi:10.1111/j.1365-2966.2010.16397.x

On the filamentary environment of galaxies

C. Gay,[1⋆] C. Pichon,[1,2] D. Le Borgne,[1] R. Teyssier,[3] T. Sousbie[1,4] and J. Devriendt[2,5]

[1]*Institut d'Astrophysique de Paris, UPMC Univ Paris 06, CNRS, UMR 7095, F-75014 Paris, France*
[2]*Department of Physics, Denys Wilkinson Building, Keble Road, Oxford OX1 3RH*
[3]*Service d'Astrophysique, IRFU, CEA-CNRS, L'orme des meurisiers, 91470 Gif sur Yvette, France*
[4]*Tokyo University, Physics Dept 7-3-1 Hongo, Bunkyo-ku, Tokyo 113-0033, Japan*
[5]*Observatoire de Lyon (UMR 5574), 9 avenue Charles André, F-69561 Saint Genis Laval, France*

Accepted 2010 January 19. Received 2009 December 18; in original form 2009 October 3

ABSTRACT

The correlation between the large-scale distribution of galaxies and their spectroscopic properties at $z = 1.5$ is investigated using the Horizon MareNostrum cosmological run.

We have extracted a large sample of 10^5 galaxies from this large hydrodynamical simulation featuring standard galaxy formation physics. Spectral synthesis is applied to these single stellar populations to generate spectra and colours for all galaxies. We use the skeleton as a tracer of the cosmic web and study how our galaxy catalogue depends on the distance to the skeleton. We show that galaxies closer to the skeleton tend to be redder but that the effect is mostly due to the proximity of large haloes at the nodes of the skeleton, rather than the filaments themselves.

This effect translates into a bimodality in the colour distribution of our sample. The origin of this bimodality is investigated and seems to follow from the ram pressure stripping of satellite galaxies within the more massive clusters of the simulation.

The virtual catalogues (spectroscopical properties of the MareNostrum galaxies at various redshifts) are available online at http://www.iap.fr/users/pichon/MareNostrum/catalogues.

Key words: hydrodynamics – methods: numerical – galaxies: evolution – large-scale structure of Universe.

1 INTRODUCTION

During the past decade, the Λ cold dark matter (ΛCDM) cosmological model of the Universe has been established as the framework of choice in which to interpret how and when observed galaxies acquire their properties. Arguably the most important feature of this framework is to provide us with an explanation as to why many of these properties (physical sizes, luminosities) strongly correlate with galaxy mass while others [star formation rates (SFRs), morphological type] do not seem to. Unsurprisingly, the all-time favoured culprit is the interplay between galaxies and the intergalactic medium (IGM) at large. In other words, the large-scale environment of galaxies is claimed to play an important role in shaping some of their properties, while the rest of them are thought to depend solely on small-scale (internal) processes. However, having said that, one still has to determine for which of these properties 'Nurture' dominates over 'Nature' and therein lies the whole difficulty of the issue.

Indeed, since the early 1970s, there has been a plethora of studies devoted to measuring the impact of environment on galaxy properties. Davis & Geller (1976) first pointed out that early-type galaxies are more strongly clustered than the late types, while Dressler (1980) and Postman & Geller (1984) demonstrated the existence of a morphology–density relation. Following in their footsteps, Balogh et al. (1998) and Hashimoto et al. (1998) and more recently Christlein & Zabludoff (2005) and Poggianti & von der Linden (2006) systematically showed that galaxies living in denser environments tend to be redder and have lower SFRs than their more isolated counterparts. One can think of several physical processes associated with different types of environment that could play a role in causing such alterations. More specifically, they include, by ascending order of environment density: (i) major (wet) mergers, which can turn spiral galaxies into ellipticals (e.g. Toomre & Toomre 1972) and drive a massive starburst wind which quenches future star formation by ejecting the interstellar medium (ISM) out of galaxies (Mihos & Hernquist 1996; Mac Low & Ferrara 1999); (ii) active galactic nuclei (AGN) or shock-driven winds (Murray, Quataert & Thompson 2005; Springel, Di Matteo & Hernquist 2005); (iii) galaxy 'harassment' (rapid encounters or flybys which dominate over mergers in rich clusters) causing discs to heat and possibly triggering the build-up of a bulge via the formation of a bar (e.g. Moore, Lake & Katz 1998). For the latter category, the diffuse gas associated with the galaxies' host dark matter (sub)halo which

⋆E-mail: gay@iap.fr

constitutes the main fuel supply for future star formation can also be stripped, thus suppressing later star formation by 'starvation' or 'strangulation' (Larson, Tinsley & Caldwell 1980; Bekki, Couch & Shioya 2002). Moreover, part of their ISM can also be pulled out of these galaxies, either by tidal forces arising from the gravitational potential of the cluster or by ram pressure stripping by the intracluster medium (ICM) (Gunn & Gott 1972; Abadi, Moore & Bower 1999; Chung et al. 2007).

Although these latter environment-dependent processes seem potent enough, recent work carried out by Tanaka et al. (2004) and van den Bosch et al. (2008) indicates that they might not be the main mechanisms for quenching star formation activity. This claim is corroborated by the higher redshift results ($z \sim 1$) obtained with the DEEP2 (e.g. Cooper et al. 2006, 2007, 2008; Gerke et al. 2007; Coil et al. 2008), (z-)COSMOS (Cassata et al. 2007; Scoville et al. 2007; Tasca et al. 2009) and VVDS (Scodeggio & Vergani 2009) surveys where clusters are more scarce, along with the fact that morphological and spectrophotometric properties of local galaxies are also found to be correlated with their internal properties, such as luminosity, mass or internal velocity (e.g. Kauffmann et al. 2003). Here as well, one can invoke various physical processes to explain such dependences on internal properties. Supernova (SN) feedback can heat and stir the ISM, possibly ejecting large amounts of gas out of galaxies, and it is expected to scale with galaxy mass (Larson 1974; Dekel & Silk 1986). There also exists a growing host of observational evidence that AGN play a key part in quenching star formation (Schawinski et al. 2006; Salim et al. 2007; Schawinski et al. 2007), and this AGN feedback should likely impact more massive galaxies since they host larger mass black holes (Magorrian et al. 1998; Silk & Rees 1998). In light of these investigations, it becomes apparent that disentangling nature and nurture is a more complicated process than one would naively have thought to begin with.

Clearly, the fundamental requirement to tackle this issue is to properly characterize the anisotropic environment of galaxies, both in observational samples and theoretical models, spanning as broad a range of environments as possible, from isolated field galaxies to groups and rich clusters. The vast majority of the studies in the literature accomplish this task either by counting the number of neighbours that a galaxy has within a fixed aperture on the sky or by measuring the distance to the nth nearest galaxy, where n is an integer in the range of 310. Although these indicators are straightforward to obtain, their physical interpretation, let alone their comparison to theoretical models, is far from being straightforward (cf. Kauffmann et al. 2004; Weinmann et al. 2006). Meanwhile, looking at the distribution of observed galaxies in modern cosmological surveys, such as the 2dF (Colless et al. 2001) and the Sloan Digital Sky Survey (SDSS; York et al. 2000), the most striking feature is that they look organized along linear structures linking clusters together (see Fig. 1). This filamentary network, dubbed as the 'cosmic web' (Bond, Kofman & Pogosyan 1996), has a dynamical origin and reflects the anisotropic accretion taking place in clusters (Sousbie et al. 2008a). It therefore seems natural to describe the environment of galaxies in terms of their location with respect to these filaments in order to investigate the influence of the cosmic web on the properties of the galaxies it encompasses.

In this paper, we carry out such a study at intermediate redshift ($z \sim 1.5$), mainly from a theoretical perspective, using a recent diagnostic tool to characterize the 3D environment called the skeleton (Sousbie, Colombi & Pichon 2009), which we combine with the largest hydrodynamical cosmological simulation performed to date (Ocvirk, Pichon & Teyssier 2008; Prunet et al. 2008; Dekel et al. 2009). Run on the MareNostrum computer at the Barcelona Supercomputer Center using the RAMSES code (Teyssier 2002), this simulation is one of the flagship simulations realized by the Horizon collaboration (http://www.projet-horizon.fr). It includes a detailed treatment of metal-dependent gas cooling, UV heating, star formation, SNe feedback and metal enrichment.

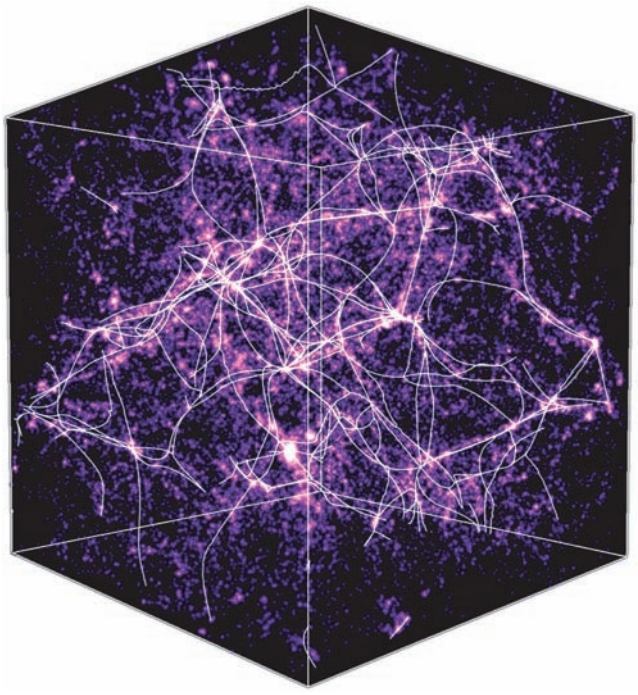

Figure 1. A 3D view of the galaxies and the skeleton of the dark matter of MareNostrum at $z = 1.6$. The box is 50 h^{-1} Mpc aside.

Specifically, we will address the question: are the physical conditions *within the filaments* dramatic enough to strongly influence the properties of the galaxies it encompasses?

The outline of this paper is as follows. First, we describe in Section 2 our methodology, in terms of numerical techniques, estimators and statistical measurements. The dependence of the spectroscopic properties on the filamentary environment is then discussed in Section 3, while Section 4 investigates the observed bimodality and discusses comparison to observations and Section 5 wraps up. Some checks are performed in Appendix A. Appendix B describes the publicly available catalogues and Appendix C sums up the subgrid physics used.

2 METHODOLOGY

Let us first describe the MareNostrum simulation, a cosmological N-body and hydrodynamical simulation of unprecedented scale which accounts for most of the physical processes involved in galaxy formation theory. The procedure to identify galaxies and assign spectra and colours to them is also described. Finally, the method used to identify filaments within the simulation is presented.

2.1 The MareNostrum simulation

We use the MareNostrum simulation, described in detail in Ocvirk et al. (2008). To summarize, this simulation uses the AMR code RAMSES(Teyssier 2002) in a periodic box of comoving 50 h^{-1} Mpc, with a ΛCDM universe ($\Omega_{\rm M} = 0.3$, $\Omega_\Lambda = 0.7$, $\Omega_{\rm B} = 0.045$,

$H_0 = 70$ km s^{-1} Mpc^{-1}, $\sigma_8 = 0.9$). The initial grid consists of 1024^3 dark matter particles ($m_{\rm part.} \simeq 8 \times 10^6\,{\rm M}_\odot$) and the same number of cells, which are refined up to five folds when they have more than eight particles, as long as the minimum cell size is not under 1 kpc in physical units. In addition to its large volume, the MareNostrum simulation provides the basic physical ingredients relevant to galaxy formation. The hydrodynamic physics uses metal-dependent cooling, UV heating [Haardt & Madau (1996) background model], star formation (Rasera & Teyssier 2006), SNe feedback and metal enrichment (Dubois & Teyssier 2008). The ISM, i.e. gas with density above 0.1 atom cm^{-3} is modelled with a polytropic equation (Schaye & Dalla Vecchia 2007) and forms stars consistently with the Kennicutt law with a star formation efficiency of 5 per cent (see Appendix C). For each snapshot, the dark matter substructures are detected with the ADAPTAH algorithm (Aubert, Pichon & Colombi 2004; Tweed et al. 2009) and all stars are associated to a (virtual) galaxy. The simulation stopped at redshift $z \approx 1.5$, with 5×10^9 cells, 1.4×10^8 star particles and around 100 000 galaxies. The simulation parameters ($L_{\rm box} = 50\,h^{-1}$ Mpc, 1024^3 dark matter particles and a spatial resolution close to $1\,h^{-1}$kpc physical) are optimal to capture the most important spectral properties of typical Milky Way like galaxies. The box size allows us to have a large sample of about 100 000 $L_\star$ galaxies at redshift 2 and above, with a strong statistical significance (see Appendix B for a detailed description of our sample).

2.2 Spectral synthesis

One main interest of the MareNostrum simulation lies in its ability to yield realistic virtual observations in a consistent cosmological framework, which in turn can be compared to real data. The outcome of these comparisons should lead to clues about the physics which drives the evolution of galaxies.

To make such predictions, light needs to be added to the simulation. This can be done very naturally by associating spectral synthesis population models to the star formation modelling in the MareNostrum simulation. More precisely, the ISM gas produces a single stellar population (SSP) per gas cell at the rate described in Section 2.1. Each of these SSPs has the metallicity of the gas which gave birth to the stars. It is described by a particle in the simulation with a mass $M\star$ (minimum value $\simeq 10^6\,{\rm M}_\odot$), a metallicity, a redshift of formation and a position. Then, we assign a dust-free *evolving* spectral energy distribution (SED) to each of these stellar particles with the PEGASE.2 (Fioc & Rocca-Volmerange 1997, 1999) population synthesis code. A Salpeter initial mass function (IMF) is used for the spectral modelling, consistently with the SN feedback.

Finally, the light content of a galaxy at redshift z is the sum of the SEDs produced by its 'stellar' (i.e. SSP) particles which depend on their age and metallicity:

$$F_\lambda(\lambda, z) = \sum_{i=0}^{n} M_i^\star \times F_\lambda^{1\,{\rm M}_\odot {\rm SSP}} \left[\lambda, t(z) - t\left(z_i^{\rm for}\right), Z\left(z_i^{\rm for}\right)\right], \qquad (1)$$

where λ is the wavelength, n is the number of stellar particles inside the galaxy, $M_i^\star$ is the total stellar mass of the ith SSP, $t(z)$ is the Hubble time at redshift z, $z_i^{\rm for}$ is the redshift of formation of the ith SSP and Z is the metallicity of the gas. Here, in contrast to the usual approximation of instantaneous mixing of chemical elements in a galaxy adopted by many models of galaxy formation [such as semi-analytic models, e.g. Hatton et al. (2003)], the simulation makes it possible to account for spatial variations of the metallicity within a galaxy. Recall that in this paper a galaxy is *defined* to be a set of at least 10 stars which are embedded within a given dark halo subclump. Rimes (2009) presents an alternative definition of a galaxy within the MareNostrum simulation based on a threshold in the baryon (gas+star) density; it was checked that both definitions yield very similar luminosity functions (LFs) at various redshifts. Appendix A4 shows that the redshift evolution of the corresponding colours seems consistent.

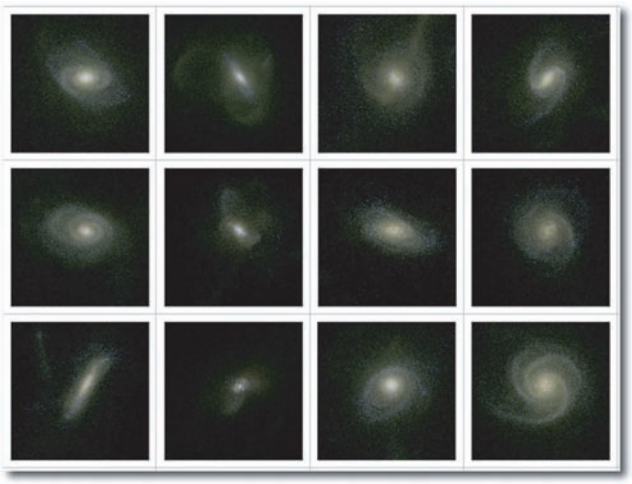

Figure 2. A sample of MareNostrum galaxies in the IRAC-8 μm, *K, I* bands which were used in this investigation. More such images are available at http://www.iap.fr/users/pichon/galaxies/.

We choose not to include reddening by dust in the predicted colours for the galaxies for two reasons. The first one is that our knowledge of dust properties and spatial distribution with respect to the gas is still somewhat uncertain. The accurate modelling of dust attenuation is a complex issue and we do not want to enter into debates regarding this modelling. The second reason is more technical: ray-tracing photons involve potentially multiple scattering, and such an approach is technically difficult to implement in a very large simulation like MareNostrum (see Devriendt et al. 2010 and Appendix A6 for an alternative approach). In the following, one must keep in mind that the effect of dust on galaxies' light is not accounted for in our work. This restriction should not impact our qualitative findings in terms of the influence of filaments, provided dust follows light, which seems a good first order approximation for this simulation (Rimes 2009 and Appendix A6).

We do include, however, IGM absorption on the line of sight, which becomes significant in optical bands at $z > 2$. We follow the prescriptions of Madau (1995) on the hypothesis of Lyα, Lyβ , Lyγ and Lyδ line blanketing, induced by H I clouds Poisson-distributed along the line of sight.

Fig. 2 shows examples of galaxies at redshift $z = 1.6$ in the MareNostrum catalogue in the *I*, *K* and IRAC-8 μm bands (see Appendix B) generated by the spectral synthesis described in this section. The consistency of these colours with classical models is checked in Appendix A4. All magnitudes are in the AB system throughout the paper. Appendix A5 carries a couple of checks on the simulation.

2.3 Filaments and the skeleton

Filaments correspond to the natural framework to characterize the environments of galaxies on large scale: within the cosmic network, large void regions are surrounded by a filamentary web linking

haloes together. Formally, the skeleton (Novikov, Colombi & Doré 2006; Sousbie et al. 2008a) gives a mathematical definition of the filaments as the locus where, starting from the filament-type saddle points (i.e. those where only one eigenvalue of the Hessian is positive), one reaches a local maximum of the field by following the gradient. This involves solving the equation:

$$\frac{\mathrm{d}\boldsymbol{x}}{\mathrm{d}t} \equiv \boldsymbol{v} = \nabla\rho\,, \tag{2}$$

for $\boldsymbol{x}$, where $\rho(\boldsymbol{x})$ is the dark matter density field, $\nabla\rho$ its gradient and $\boldsymbol{x}$ the position. Finding the large-scale structure network of filaments involves solving equation (2), a procedure which has recently been applied to both data (Sousbie et al. 2008b) and simulations (Caucci et al. 2008). A similar approach is to classify the different structures (haloes, filaments, sheets and voids) according to the eigenvalues of the Hessian of the density field (Aragón-Calvo et al. 2007) or the potential (Pogosyan et al. 1998; Hahn et al. 2007; Forero-Romero et al. 2009).

Recently, Sousbie et al. (2009) introduced a probabilist formulation of the skeleton, which amounts to finding the solution to equation (2) at the intersection of the void patches of the density field. The filaments can then be seen as the frontiers between the voids. This algorithm has the nice feature of constructing a fully connected network of critical lines, a crucial feature for this project. The implementation of this algorithm on the density field of MareNostrum, with a smoothing[1] over 2 h^{-1} Mpc yields a hierarchical set of segments, where each skeleton segment tracks its connection to its neighbouring critical points, together with information relative to the underlying field (density, temperature, etc). The result is illustrated in Fig. 1 where one can see that the skeleton smoothed on these scales traces well the large-scale overdense filaments, visible by eye.

3 THE INFLUENCE OF FILAMENTS

The combination of the MareNostrum simulation with spectral synthesis and the skeleton algorithm allows us to investigate the *geometric* dependence of the spectroscopic properties of galaxies on the filamentary environment.

3.1 Gradient of physical properties

To investigate the influence of filaments on the properties of the galaxies, we choose to study the colours in the observer frame as a function of the distance to filaments. The locus of the filaments (shown in Fig. 1) is computed with the above-described skeleton algorithm, using a 256^3 grid and smoothing on $\sigma = 12$ pixels (i.e. 2 h^{-1} Mpc). Fig. 3 represents the distribution of the observed colour $G - K$ (which brackets the 4000 Å break in the SED at this redshift) as a function of distance to large-scale filaments. First, independently to the distance to filaments, the distribution in colour shows a bimodality that will be investigated in further details in Section 4: a distinct population of very red galaxies is present. Then it also shows that galaxies tend to be redder near filaments. The trend is clearly seen when the distribution is averaged (Fig. 4): the $G - K$ colour drops from 2.1 near filaments to 1.7 at a distance of 5 h^{-1} Mpc. Galaxies exhibit a clear gradient of colour versus the distance to filaments.

[1] See Appendix A2 for a discussion on the effect of smoothing on the results presented here.

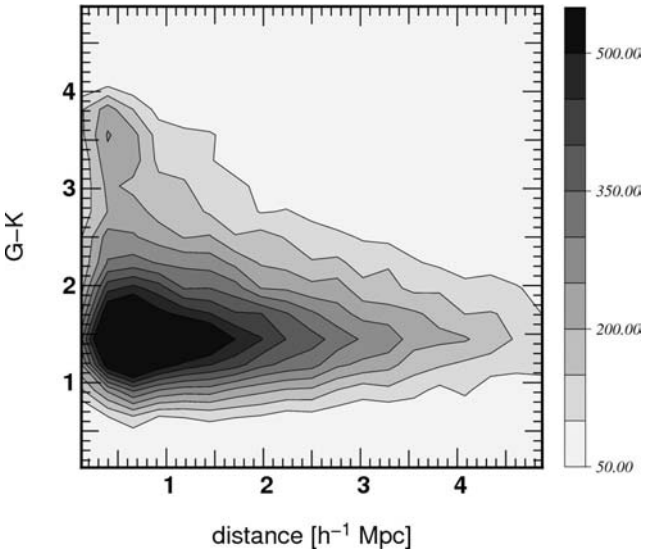

Figure 3. Isocontours of the number counts of galaxies in observed colour versus distance to filament space at redshift $z = 1.6$. A population of redder galaxies is present in the close vicinity of the filaments.

3.2 On the influence of nodes and filaments

The interpretation of this gradient is not straightforward since the distance to the skeleton does not only reflect the influence of filaments. Indeed, clusters, located at the nodes of the skeleton, have been known (e.g. Goto et al. 2004 and references therein) to have a strong influence on the properties of the galaxies. Galaxies near filaments are also geometrically systematically closer to nodes, and this bias could explain the observed gradient.

The same procedure can be applied to the distance to the nodes alone (Fig. 5). The influence of nodes on the colours turns out to be even greater than the effect of the distance to filaments; it may thus explain a major part of the dependence of the colour with the distance to filaments.

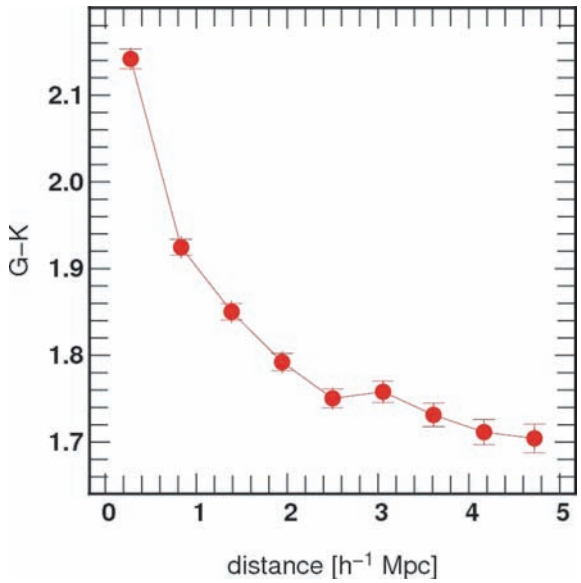

Figure 4. Average observed colour as a function of distance to the closest filament at $z = 1.6$. The error bars, for all the figures, represent the 1σ error on the average. Galaxies near filaments tend to be redder on average than galaxies located a few megaparsecs away from filaments.

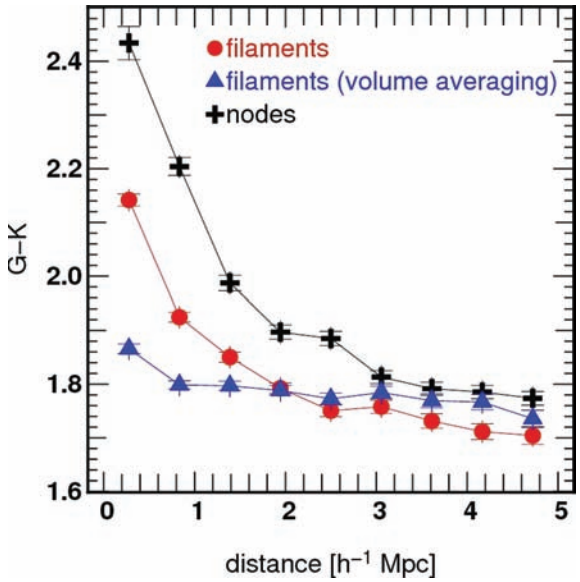

Figure 5. Circles: average colour versus distance to the closest filament at $z = 1.6$. Triangles: volume averaging. Crosses: distance to nodes. The gradient of colour as a function of distance to filaments can be mostly explained by the sole influence of the nodes and is strongly damped when focusing on the filaments.

One can however decrease relatively the contribution of the nodes by using a volume average rather than a number average:

$$\langle x \rangle_{\rm vol} = \sum_i \frac{1}{\rho_i} x_i \Big/ \sum_i \frac{1}{\rho_i}, \tag{3}$$

where ρ_i is the density of galaxies at the position of the ith galaxy. Nodes contain most of the galaxies and are therefore overrepresented with number-averaged weighting, while volume-weighted means will shift the focus on the filaments, which span on much greater scales than clusters. The volume-averaged colour is plotted against the distance to the filaments in Fig. 5. The colour gradient is strongly damped, showing that most of it can be explained by the bias corresponding to the distance to nodes.

Even if the influence of nodes is greatly reduced by volume averaging, it does not totally vanish; it makes it difficult to rule out a weak influence of filaments relative to a residual influence of nodes. One would want to know how the properties of a galaxy would be modified if its distance to filaments was changed while all other parameters, including the distance to nodes, are kept unchanged. A way to evaluate this is to look at galaxies having the same distance to nodes but different distances to filaments. In order to find such pairs of galaxies, we proceed in steps (Fig. 6). For each galaxy, we first look at the closest skeleton segment ($G \triangleright S$). This segment being closer to nodes, we follow the filament until we reach a segment with a distance to the node sufficiently close to the distance between the node and the initial galaxy ($S \triangleright N \triangleright S'$). The closest galaxy to this segment is considered to be the filament counterpart of the initial galaxy ($S' \triangleright G'$): it has roughly the same distance to the node, but is generally much closer to the filament. The comparison of a galaxy and its filament counterpart is therefore of much interest to study the influence of the sole filaments. Note that this construction is not always possible. Indeed if two nodes are quite close, and if the initial galaxy is far from the filament, the filament linking them is too short to find a segment equating the distance to the node. Therefore, some galaxies do not have filament counterparts and are rejected.

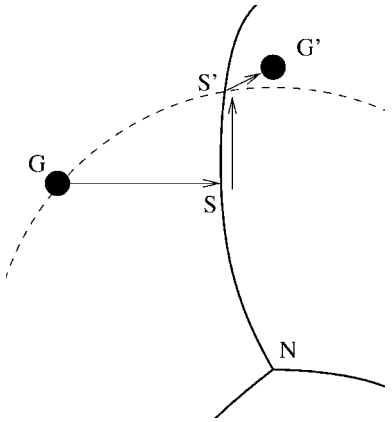

Figure 6. Illustration of the algorithm used to find the filamentary counterparts. For each galaxy G, we find the closest skeleton segment S. We follow the skeleton until the point S' where the distance to the node N is sufficiently close to the distance between G and N. Then the closest galaxy G' is found and labelled as the filament counterpart of G. A galaxy and its filament counterpart have approximately the same distance to the node, but the filament counterpart is generally much closer to the filament. Thus, it opens the possibility of unbiased comparison.

If we accept only the galaxies whose counterpart has a distance node greater than 90 per cent of the distance of the initial galaxy, around two thirds of the galaxies have a filament counterpart. Note, however, that the galaxies rejected are, as explained, far from small filaments, while the galaxies close to important filaments, which are of interest in our investigation, should not be affected. Fig. 7 shows the difference of colour between a galaxy and its counterpart. When this procedure is implemented no significant statistical difference is found, showing that the influence of the filaments is too weak to be detected by this method and that the small gradient exhibited by the volume averaging procedure can be for the most part explained as a residual influence of the nodes.

3.3 Other physical tracers

The physical properties studied in the previous section are the observed colours, since they are easy tracers to observe and are known to reflect well the other properties of the galaxies. For the MareNostrum simulation, the same procedure can however be applied to other physical intrinsic features of galaxies. Fig. 8 shows the trend for the rest-frame colour UV-I, the specific SFR, SFR/M_*, and the

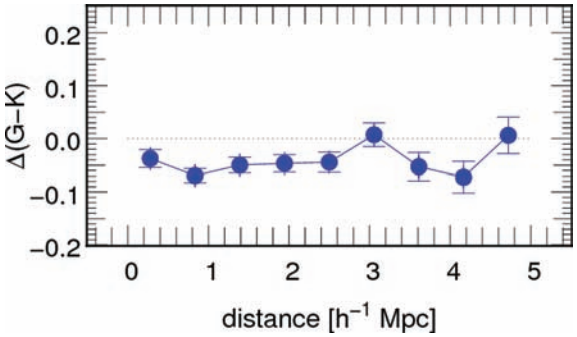

Figure 7. Difference of observed colour between the galaxies and their filament counterparts versus distance to the closest filament. Even though a residual 2σ shift from zero remains, no overall gradient is present. Galaxies far from filaments do not tend to be different from their filament counterpart.

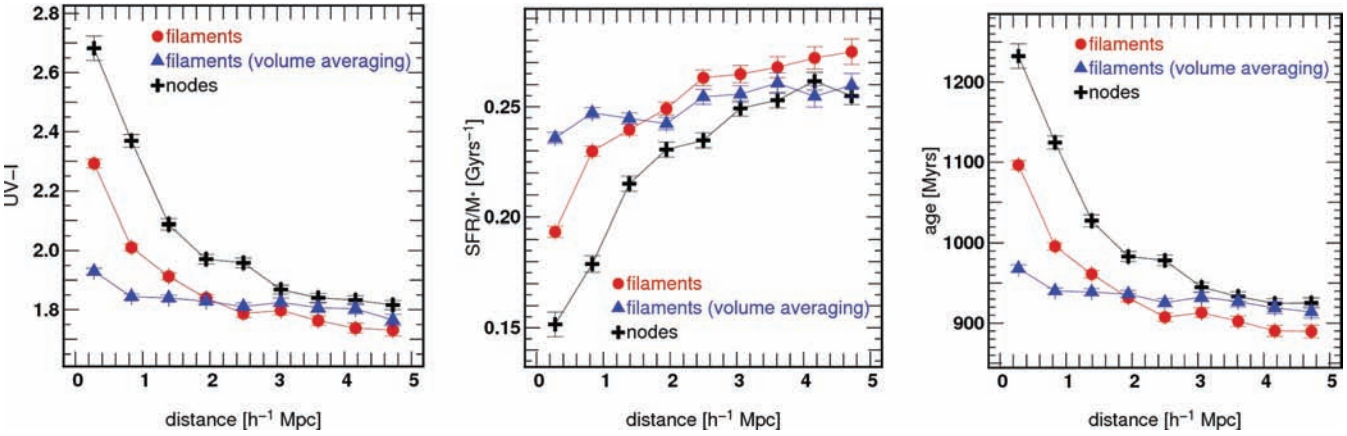

Figure 8. Same as Fig. 5 for UV-I rest-frame colour (left-hand panel), specific SFR (middle panel) and mean light-weighted stellar age (right-hand panel). As expected, the same trends are found for these physical tracers as for the intrinsic colours.

galaxy mean stellar age. As for the observed colour, no statistically significant gradient remains once the influence of nodes is properly removed.

Fig. 9 shows the trend for the metallicity. A gradient is still present after volume averaging and can be seen in pair comparison. The filaments seem to have an influence on the metallicity of the galaxies: the closer to the filaments the galaxies are, the more metallic they are. This gradient is however fairly small (0.1 dex is the order of magnitude of the global change in the metallicity of galaxies within 1 Gyr at this epoch; see Savaglio et al. 2005), which is consistent with the fact that the other properties, which are indirectly related to metallicity, do not exhibit any significant gradient. This gradient may nevertheless reflect the enrichment of the warm–hot intergalactic medium (WHIM; Cen & Ostriker 1999). Indeed, it is a consequence of the increased galaxy density, together with the corresponding (in-)efficiency of winds as induced by the subgrid physics. If this result were confirmed not to depend critically on the SNe rate recipe, it offers the prospect of directly exploring this component of the IGM via the metallicity of galaxies. It would then be of interest to cross-correlate this metallicity with that of the O_{IV} absorbers (Yoshikawa et al. 2003).

4 BIMODALITY WITHIN CLUSTERS

In addition to its evolution with the distance to filaments, the presence of a bimodality corresponds to an interesting feature of the distribution of colours: as seen in Fig. 3, a population of very red galaxies ($G - K > 3$) is present. Moreover, the evolution of the colour distribution with redshift shows that this bimodality is appearing around $z = 2$ (Fig. 10). Let us therefore trace back the positions of galaxies responsible for this bimodality in order to explain its origin.

4.1 Properties of the reddest galaxies

Fig. 11 shows the distribution of distance to nodes for the reddest galaxies ($G - K > 3$) and for the overall sample. Red galaxies are shown to be more clustered near nodes.

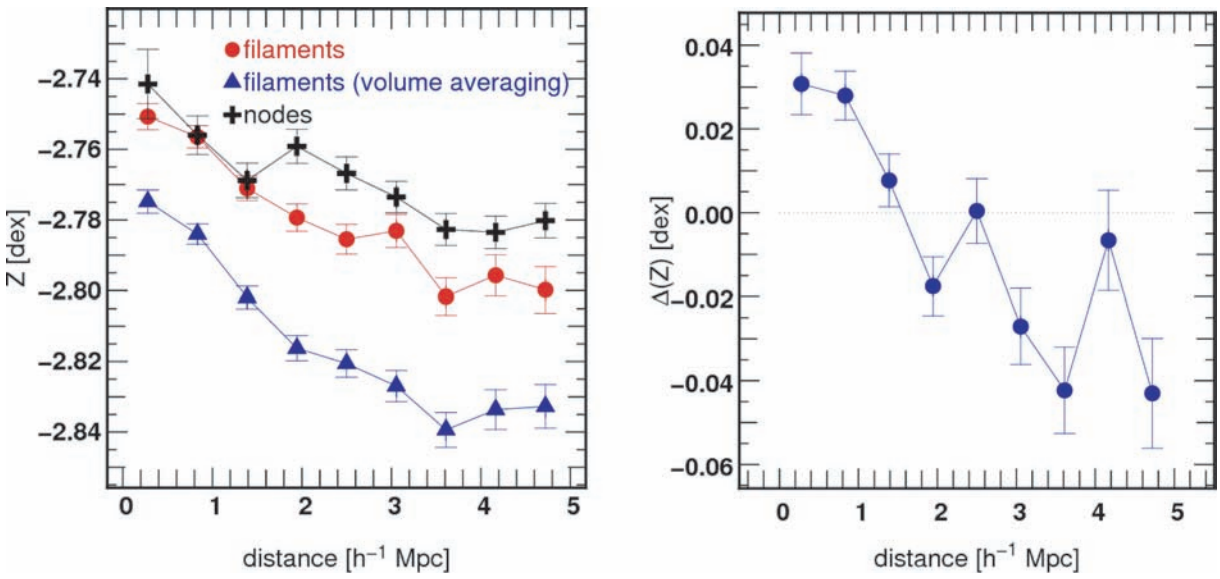

Figure 9. Same as Fig. 5 (left-hand panel) and Fig. 7 (right-hand panel) for the metallicity. Metallicity shows a clear gradient as a function of distance to filaments. This gradient reflects the inhomogeneity of the WHIM on these scales for the MareNostrum subgrid physics.

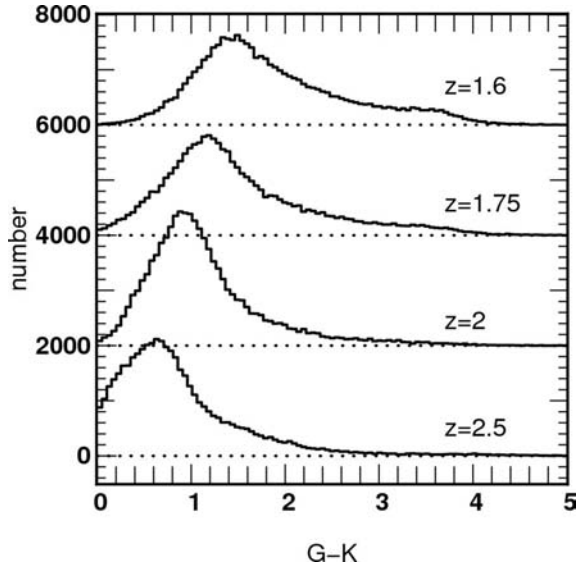

Figure 10. Distribution of observed colour for several redshifts ($z = 1.6$, 1.75, 2.0 and 2.5). The curves are shifted by 2000 for clarity. Note the weak bimodality occurring below redshift 2.

These red galaxies also exhibit a very low mass ($M \sim 10^8\,\mathrm{M}_\odot$). Indeed, as Fig. 12 shows, the galaxies are either blue (with high or low masses) or red with low masses. Such small masses associated to very red colours (which in our case mean an absence of star formation since we do not include internal dust in the modelling of the SEDs) suggest that these may be dwarf spheroidals, which origin is still poorly known. Grebel, Gallagher & Harbeck (2003), in a study of dwarf galaxies in the Local Group, suggested that the absence of star formation in such objects is due to externally induced gas loss: ram pressure stripping would be responsible for lack of ISM gas in these small galaxies. Mayer et al. (2007) showed that stripping in the clusters can indeed increase the mass-to-light ratio of dwarf galaxies. It is possibly the case here too, as demonstrated in Section 4.2 and Fig. 13. In contrast to what is observed

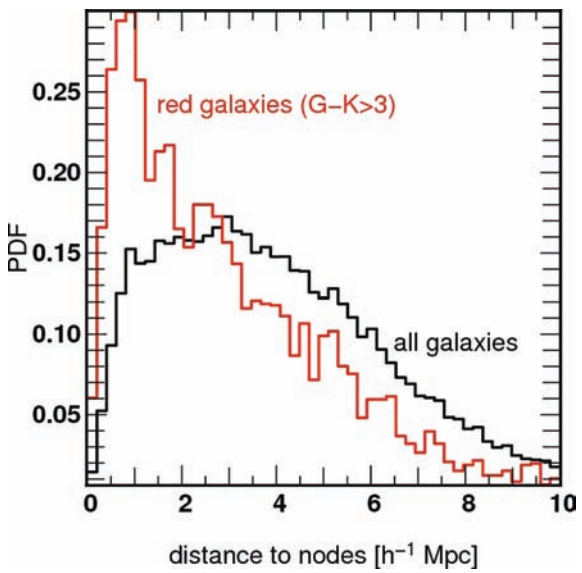

Figure 11. PDF of the distance to nodes for all galaxies (black) and reddest ($G - K > 3$) galaxies (red). The reddest galaxies are clustered near the nodes.

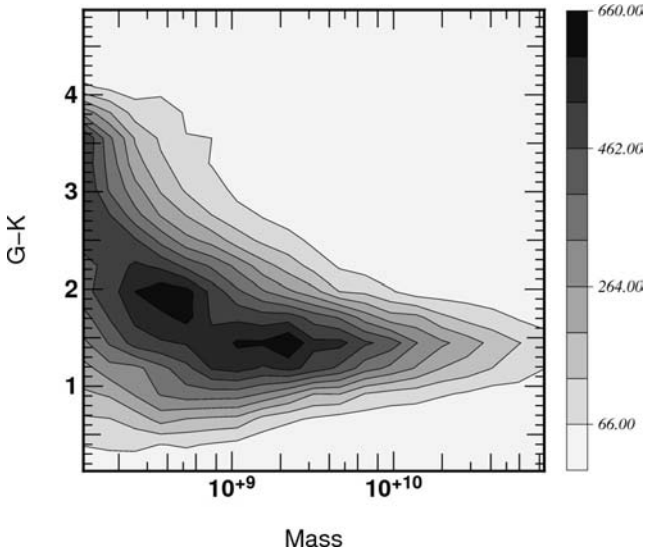

Figure 12. Isocontours of the density of galaxies in mass versus colour space, for $z = 1.6$. Red galaxies are typically less massive.

at low redshift, there is no massive red galaxy in the simulation at $z = 1.6$.[2]

4.2 Dynamical scenario

The dependence of the spectrophotometric properties with the distance to filaments studied in the previous sections reflects the process of galaxy formation and its connection with the global flow within the large-scale structure. Indeed, it has been demonstrated (Aubert et al. 2004; Sousbie et al. 2008a) that filaments are fed by surrounding voids and mark the lanes of galactic infall towards the clusters. Young galaxies form across the whole filamentary network, but are rapidly collected along the more busy subnet of denser filaments.

A close-up look at a specific halo (see Fig. 13) confirms the presence of small, red galaxies (which do not form stars) embedded in the halo. These galaxies are already accreted at $z = 2$. At this range of redshift, haloes contain big ($M > 10^{10}\,\mathrm{M}_\odot$), blue, central galaxies and small ($M < 10^9\,\mathrm{M}_\odot$), red galaxies which are being stripped of their gas and swallowed by the central galaxy. The fate of these small galaxies can be investigated by looking to another population: the galaxies that are currently accreting into the haloes at this epoch, although they have a larger mass ($10^9\,\mathrm{M}_\odot < M < 10^{10}\,\mathrm{M}_\odot$). These intermediate galaxies show a peculiar behaviour that could explain the observed increase of the average colour near nodes: when approaching the halo, they stop forming stars and therefore begin to passively redden. This quench could be triggered by the lack of cold stream reaching the inner core of dark haloes (Ocvirk et al. 2008) or by stripping of their gas (Moore, Quilis & Bower 2000). Ocvirk et al. (2008) show that more massive haloes prevent cold stream from feeding the inner halo; here it is found that these haloes display redder satellites. The accreted galaxies tend therefore to be red and have a low SFR, leading to the previously observed bimodality.

[2] Low-mass galaxies should be considered with caution in such a simulation. For instance low-mass galaxies are expected to be artificially blue as they only have a recent accretion history, whereas more massive galaxies are spectrally better resolved. However, this effect would not explain the fact that the galaxies studied are redder.

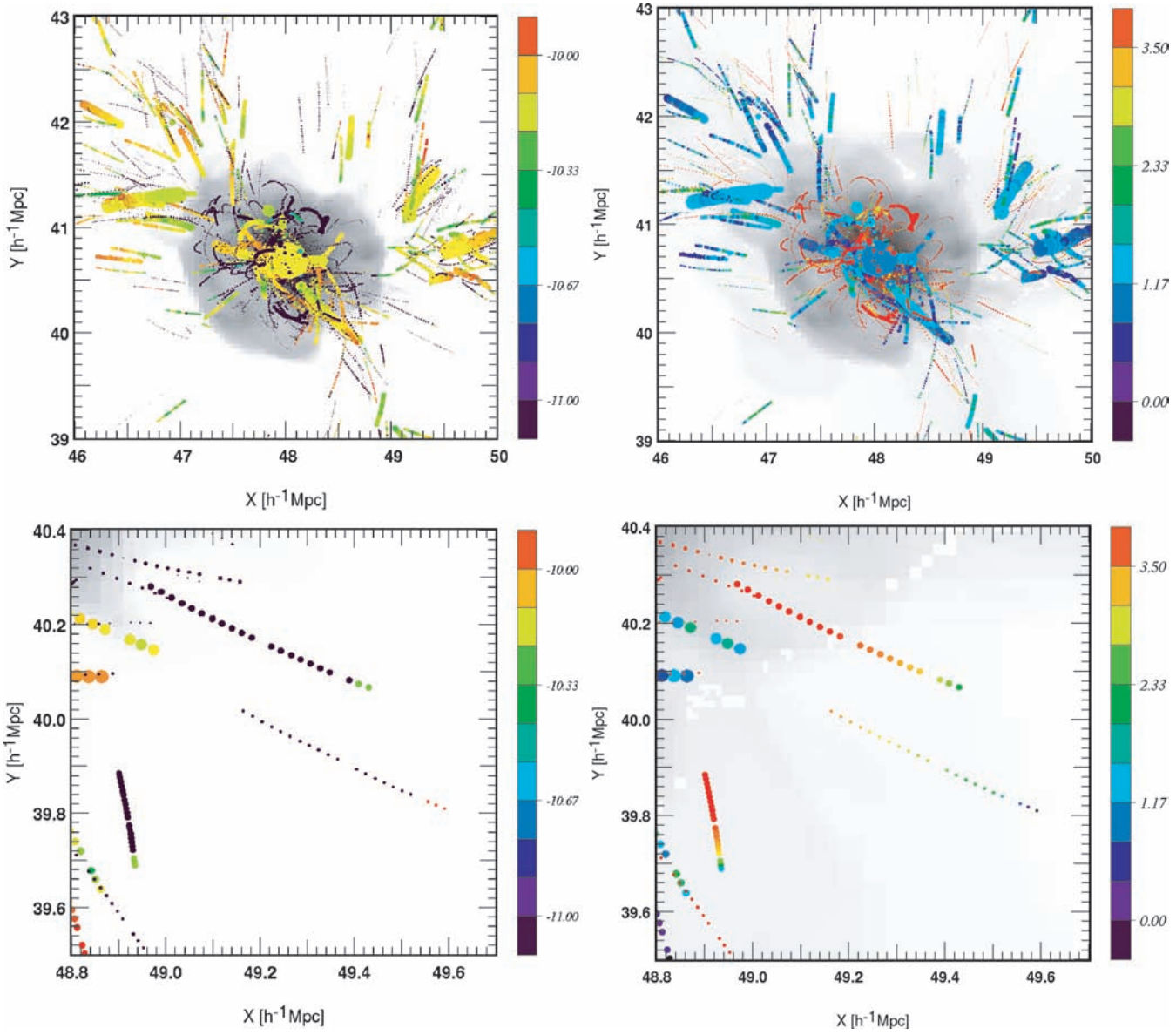

Figure 13. View of a small region of the simulation centred on a large cluster. The traces represent the position of the galaxies for several time-steps between $z = 1.9$ and 1.6. Each galaxy is represented by a point whose size depends on its mass and whose colour represents either the SFR/M_* (left-hand panel) or the UV-I rest-frame colour (right-hand panel). The top figures represent a 4 h^{-1} Mpc cube and the bottom ones are a zoom on the bottom-right part and span over 1 h^{-1} Mpc. The grey background encodes the temperature of the gas, showing the extent of the hot gas bubble. Note the reddening of the small galaxies entering the cluster (bottom right), in parallel to the reduced star formation (bottom left).

They would then merge with the central galaxies and contribute to the increase in mass (dry merging) of the massive old galaxies observed at low redshift.

In this scenario, the spectroscopic properties of a galaxy should be at least in part determined by the physical conditions of the ICM. Figs 14 and 15 are consistent with this scenario. Indeed the average colour increases with the pressure, as expected in the case where the reddening is induced by star formation quenching via ram pressure stripping. The detailed 2D distribution shows the presence of a population of very red galaxies for high pressures. These galaxies could correspond to the galaxies which have been stripped of their gas when they entered the cluster and will then become red, small galaxies, before they eventually merge with the core galaxies.

The typical pressure of transition is around 10^{-14} Pa and corresponds to conditions found only near nodes (see Fig. 16). Theoretical considerations and simulations (Fujita & Nagashima 1999; Roediger 2009) show that ram pressure stripping is expected to be efficient for pressure over 10^{-13} Pa. This apparent discrepancy may be explained by noticing that we are considering different objects. Their value corresponds to the pressure required to strip a typical spiral galaxy at low redshift and could thus be lower for the smaller high redshift galaxies we are considering.

4.3 Tentative link with observations

It is clearly beyond the scope of this paper to carry a direct comparison with the currently available data. Indeed, the main difficulty in comparing the results found in this simulation with existing observations lies in the range of redshifts and the geometry of the surveys. Building a fully connected skeleton is non-trivial for pencil shape

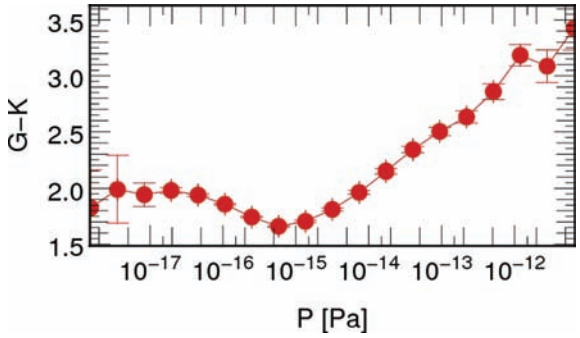

Figure 14. Mean observed colour, $G - K$, as a function of pressure of the galaxy. Galaxies are redder in high-pressure regions.

volumes, as edge effects become important (as discussed in Sousbie et al. 2008a). Moreover, in this paper, the skeleton was computed from the dark matter distribution and one would need to calibrate the bias involved in using light instead of mass.

Finally, the simulation was stopped at $z \approx 1.5$, and the bimodality seems to appear around $z \approx 2$ (see Fig. 10). Observations at such high redshift are uncommon and difficult (Daddi et al. 2005; van Dokkum et al. 2006). However, as mentioned in Section 1, similar trends exist for the same range of redshift: for example, red galaxies are observed to be more clustered (Daddi et al. 2003).

These gradients can also be linked to slightly lower redshift observations. For redshift $z \approx 1$, there exists several surveys that have studied the role of the environment, e.g. GOODS (Elbaz et al. 2007), VVDS (Scodeggio & Vergani 2009) or DEEP2 (Cooper et al. 2006). The existence of a bimodality, with a blue and a red sequence, is known to appear at this redshift (Nuijten et al. 2005) and can be observed on several properties of galaxies at low redshift (Mouhcine, Baldry & Bamford 2007).

To better understand the link with observations, one has to understand the robustness of the results with respect to observational uncertainties and other biases. The nature of this virtual data set allows us to compute directly the properties (skeleton,

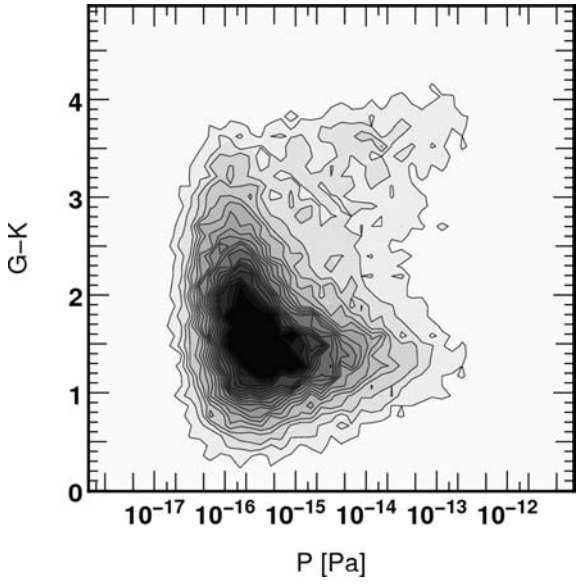

Figure 15. Distribution of galaxies in observed colour ($G - K$) pressure space. The increase of the $G - K$ colour with pressure is due to a distinct population.

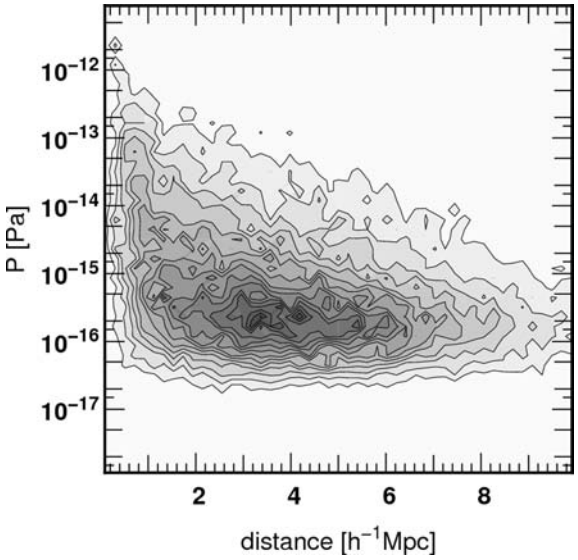

Figure 16. Pressure of the galaxies versus distance to nodes. High pressures (likely to strip low-mass galaxies of their gas) are only found near massive clusters.

distance to filaments, ...) in 3D, without any problems of distance determination. For observational applications, a natural question arises: are these results robust with respect to distance uncertainty that can come, e.g., from the use of photometric redshifts (Cooper et al. 2005)? In order to asses this robustness, the simulation cube is projected along one of its axis. The 50 h^{-1} Mpc can be thought of as representing the uncertainty on distance (roughly $\delta z = 0.005$ at $z = 1.6$). A 2D skeleton is computed on the resulting density field, with the same N-dimensional algorithm. The observed colour is then compared to the 2D distance to the closest filament (see Fig. 17). The main features found in the 3D investigation are still weakly present after projection: a distinct population can be seen near nodes and leads to an enhanced averaged colour, but filaments do not seem to have an effect on the properties of the galaxies. This effect is however far more subtle than in 3D, given the projection effect.

Finally, as an alternative to the skeleton as a tracer of filaments let us briefly implement a few more commonly used tracers (as mentioned in the Introduction) on the MareNostrum simulation: the 2D distance to the 5th neighbour (Cooper et al. 2005) and the galaxy number density. Fig. 18 shows that a bimodality is still present with the 5th neighbour probe, but it is much less contrasted and much more localized. The 2D distance to the 5th neighbour is therefore a less sensitive probe of the anisotropic cosmic environment. In

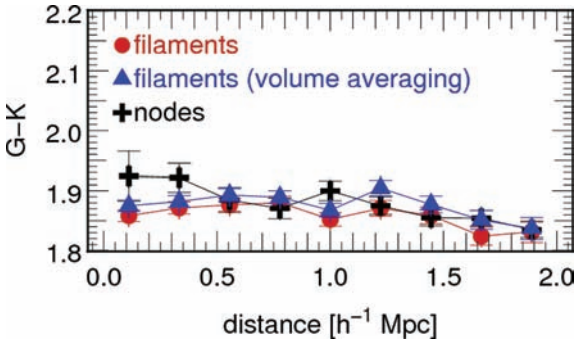

Figure 17. Same as Fig. 5 for the 2D skeleton. A weak trend is still present but much less significant than in 3D.

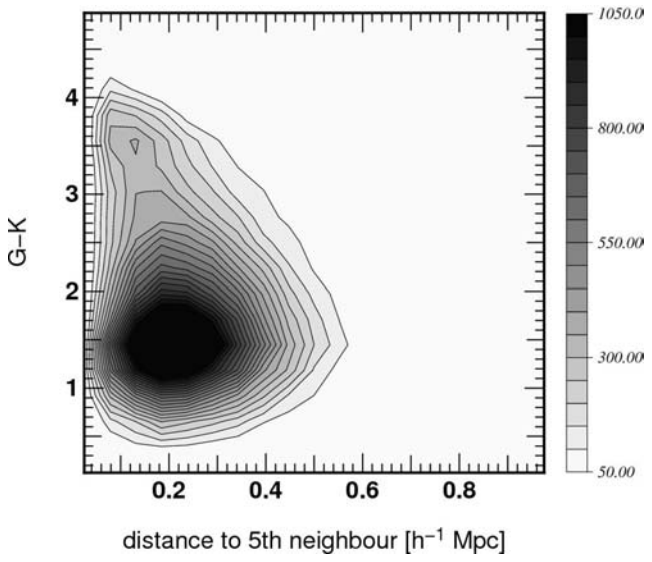

Figure 18. Isocontours of the number count of galaxies in observed colour versus distance to the 5th neighbour for the projected data at $z = 1.6$. Note the larger number of contours used to catch the low-contrast bimodality, compared to Fig. 3. Note also the difference of scale on the x axis: the 5th neighbour does not probe large-scale structures when no cut on galactic mass is applied.

contrast, provided spectroscopic redshifts are available (say with the LSST; Claver et al. 2004), the 3D skeleton should allow us both to probe the large-scale structures and mark the neighbourhood of clusters in detail.

Finally, Fig. 19 shows that the bimodality is not present anymore when the galaxy number density is used, in 2D or 3D.

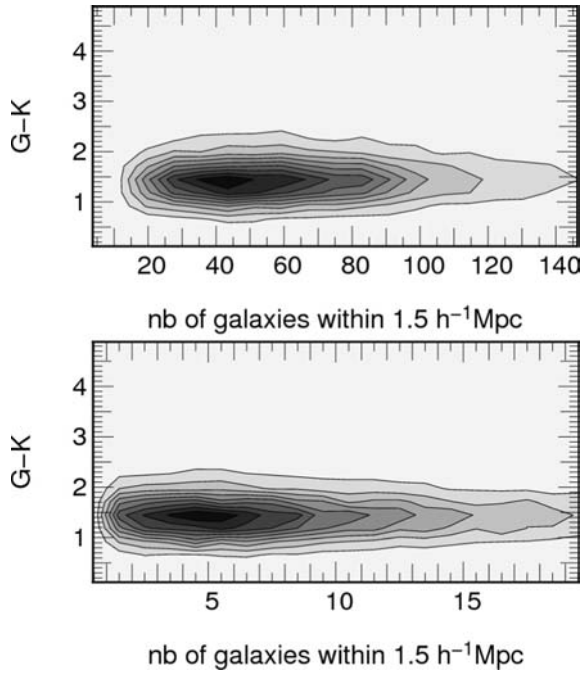

Figure 19. Isocontours of the number count of galaxies in observed colour versus number of galaxies within a sphere of 1.5 h^{-1} Mpc for the projected data (top panel) and the 3D data (bottom panel). No significant trend is seen with these classical tracers.

5 CONCLUSION AND DISCUSSIONS

The cosmic web is a key feature of the organization of galaxies on large scales. This paper investigated the influence of this filamentary environment on the spectroscopic properties of galaxies, using the MareNostrum simulation which was postprocessed using stellar population synthesis. The cosmic web was traced with the skeleton algorithm and has proven here to be a very effective mean of probing the anisotropy of the large-scale structures.

We found gradients of spectroscopic properties of galaxies with the distance to filaments but demonstrated that they can be explained by the fact that the distance to filaments is biased by the distance to the nodes of the network (group or clusters of galaxies). Two procedures were introduced to remove the influence of these nodes: (i) volume averaging this distance decreases the influence of the compact, dense regions and focus on wider structures, such as filaments; (ii) pair comparison which seeks the filamentary counterpart of each galaxy. Both methods show that the influence of the filaments alone is negligible compared to influence of clusters. A bimodality in colour was also found to occur below redshift $z \approx 2$, and its origin was investigated. It is due to a population of red, small galaxies ($\sim 10^8\,M_\odot$) accreting on the nodes of the cosmic web, while more massive objects, $M > 10^8\,M_\odot$, are mostly unaffected. These galaxies have their star formation quenched while they approach the clusters. It remains to be confirmed that this stripping process is not amplified by a lack-of-resolution effect, since (i) it involves amongst the smallest (virtual) galaxies in the simulation, and (ii) it seems to create a tension with observations at redshift zero (Kimm et al. 2009).

These findings suggest that the large-scale filaments are only dynamical features of the density field, reflecting the flow of galaxies accreting on clusters; the conditions in the filaments are not dramatic enough to influence strongly the properties of the galaxies it encompasses, unlike the intra (proto) cluster medium, which seems able to strip down the ISM of the incoming low-mass galaxies. Appendix A3 shows that this statement remains valid when the study is limited to the most important filaments.

Finally, we did find a weak metallicity gradient away from the filaments which could reflect the large-scale inhomogeneity in the distribution of metals (the so called WHIM).

One could have imagined that even if the large-scale filamentary network were purely a tracer of the large-scale dynamics, galaxies within the large-scale filaments should be redder and older, since they would have joined the cosmic super highway earlier on average when compared to field galaxies. This effect is not seen at those redshifts, as (i) older galaxies continue to accrete new cold gas on small scales and form stars, hence remain blue, (ii) some field galaxies continuously join the large filamentary network and (iii) on large scales, a significant fraction of the matter is accreted more or less radially on to the nodes, while filaments are collecting leftovers from this accretion more indirectly (Sousbie et al. 2008a).

Recently (Kereš et al. 2005; Ocvirk et al. 2008; Dekel et al. 2009), it was emphasized in steps that anisotropic metal-rich cold stream accretion regulates the inflow of cold gas towards the inner regions of the most massive galaxies of the high-redshift universe ($z > 2$). It was then conjectured that this process could explain the observed bimodality of spectroscopic galactic properties at lower redshift. In this paper, we have shown that the geometric distribution of the colour of galaxies is not sensitive to the detailed large-scale filamentary network, but only to its nodes. This apparent paradox may be lifted when noting that the self-regulating anisotropic filamentary accretion occurs on much smaller scales and was quantified for the

central galaxies of the simulation which *are* sitting at the nodes of the network; in contrast, when considering the full galactic population, a typically low-mass galaxy is not transformed by its encounter with the different physical condition of the weakly overdense IGM within the cosmic web, unless it falls into the ICM of a large node.

In other words, massive galaxies feel the small-scale filaments (cold streams) feeding them at nodes; low-mass galaxies are not spectroscopically changed while entering the large-scale filaments. The mesoscopic (below an Mpc scale) filamentary feature of the cosmic network may geometrically solve the self-regulating process of galactic accretion, but we have demonstrated here that its large-scale counterpart does not seem to directly affect the colours of galaxies.

In Sousbie et al. (2009), the effect of redshift distortion is partially addressed, and the corresponding algorithm is now being extended to discrete surveys via a Delaunay tessellation (which are therefore not sensitive to edge effects). This, as argued in Section 4.3 is a critical step towards performing a similar 3D analysis on real data, which as we have shown is essential to quantify these gradients, as in projection, the information is lost (see Fig. 17). In particular, it would be of great interest to carry out these measurements on a DEEP-2/VVDS/z-COSMOS-like survey as well as to bring the simulation down to lower redshift and reach a time in cosmic history when upcoming large observational surveys (e.g. LSST, Claver et al. 2004; BOSS, Schlegel 2007) overlap statistically with the predictions of the simulation. It would also be worth investigating how sensitive some of our findings are with respect to the detailed chosen subgrid physics by probing alternative recipes and running higher spatial resolution simulations.

The catalogues produced for this investigation (spectroscopical properties of the MareNostrum galaxies and its dark matter skeletons) are available online as discussed briefly in Appendix B.

ACKNOWLEDGMENTS

We thank F. Brault for her help in a preliminary investigation and S. Colombi, D. Pogosyan, Y. Dubois and D. Aubert for fruitful comments during the course of this work. This investigation was carried within the framework of the Horizon project, www.projet-horizon.fr. The simulation was run on the MareNostrum machine at the Barcelona Supercomputing Centre, and we would like to warmly thank the staff for their support and hospitality. We also thank D. Munro for freely distributing his Yorick programming language and OpenGL interface (available at http://yorick.sourceforge.net/). CP thanks the Leverhulme Trust for the visiting professorship F09846D.

REFERENCES

Abadi M. G., Moore B., Bower R. G., 1999, MNRAS, 308, 947
Aragón-Calvo M. A., Jones B. J. T., van de Weygaert R., van der Hulst J. M., 2007, A&A, 474, 315
Aubert D., Pichon C., Colombi S., 2004, MNRAS, 352, 376
Balogh M. L., Schade D., Morris S. L., Yee H. K. C., Carlberg R. G., Ellingson E., 1998, ApJ, 504, L75
Bekki K., Couch W. J., Shioya Y., 2002, ApJ, 577, 651
Bond J. R., Kofman L., Pogosyan D., 1996, Nat, 380, 603
Bouwens R. J., Illingworth G. D., Franx M., Ford H., 2007, ApJ, 670, 928
Calzetti D., 2001, PASP, 113, 1449
Cassata P. et al., 2007, ApJS, 172, 270
Caucci S., Colombi S., Pichon C., Rollinde E., Petitjean P., Sousbie T., 2008, MNRAS, 386, 211
Cen R., Ostriker J. P., 1999, ApJ, 514, 1
Christlein D., Zabludoff A. I., 2005, ApJ, 621, 201
Chung A. et al., 2007, in Spitzer Proposal ID #40784 Cluster Environmental Effects on Galaxy Evolution at z = 0.2 (Abell 963 vs. Abell 2192). p. 40784
Claver C. F. et al., 2004, in Oschmann J. M., Jr, ed., Society of Photo-Optical Instrumentation Engineers (SPIE) Conf. Ser. Vol. 5489, Project Status of the 8.4-m LSST. SPIE, Bellingham, p. 705
Coil A. L. et al., 2008, ApJ, 672, 153
Colless M. et al., 2001, MNRAS, 328, 1039
Cooper M. C., Newman J. A., Madgwick D. S., Gerke B. F., Yan R., Davis M., 2005, ApJ, 634, 833
Cooper M. C. et al., 2006, MNRAS, 370, 198
Cooper M. C. et al., 2007, MNRAS, 376, 1445
Cooper M. C. et al., 2008, MNRAS, 383, 1058
Daddi E. et al., 2003, ApJ, 588, 50
Daddi E. et al., 2005, ApJ, 631, L13
Davis M., Geller M. J., 1976, ApJ, 208, 13
Dekel A., Silk J., 1986, ApJ, 303, 39
Dekel A. et al., 2009, Nat, 457, 451
Devriendt J. et al., 2010, MNRAS, 403, L84
Dressler A., 1980, ApJ, 236, 351
Dubois Y., Teyssier R., 2008, A&A, 477, 79
Elbaz D. et al., 2007, A&A, 468, 33
Fazio G. G. et al., 2004, ApJS, 154, 10
Fioc M., Rocca-Volmerange B., 1997, A&A, 326, 950
Fioc M., Rocca-Volmerange B., 1999, preprint (astro-ph/9912179)
Forero-Romero J. E., Hoffman Y., Gottlöber S., Klypin A., Yepes G., 2009, MNRAS, 396, 1815
Fujita Y., Nagashima M., 1999, ApJ, 516, 619
Fukugita M., Ichikawa T., Gunn J. E., Doi M., Shimasaku K., Schneider D. P., 1996, AJ, 111, 1748
Gerke B. F. et al., 2007, ApJ, 660, L23
Goto T., Yagi M., Tanaka M., Okamura S., 2004, MNRAS, 348, 515
Grebel E. K., Gallagher J. S. III, Harbeck D., 2003, AJ, 125, 1926
Gunn J. E., Gott J. R. I., 1972, ApJ, 176, 1
Haardt F., Madau P., 1996, ApJ, 461, 20
Hahn O., Carollo C. M., Porciani C., Dekel A., 2007, MNRAS, 381, 41
Hashimoto Y., Oemler A. J., Lin H., Tucker D. L., 1998, ApJ, 499, 589
Hatton S., Devriendt J. E. G., Ninin S., Bouchet F. R., Guiderdoni B., Vibert D., 2003, MNRAS, 343, 75
Hopkins A. M., Beacom J. F., 2006, ApJ, 651, 142
Johnson H. L., Iriarte B., Mitchell R. I., Wisniewskj W. Z., 1966, Commun. Lunar Planet. Lab., 4, 99
Kauffmann G. et al., 2003, MNRAS, 341, 54
Kauffmann G., White S. D. M., Heckman T. M., Ménard B., Brinchmann J., Charlot S., Tremonti C., Brinkmann J., 2004, MNRAS, 353, 713
Kennicutt R. C., Jr, 1998, ApJ, 498, 541
Kereš D., Katz N., Weinberg D. H., Davé R., 2005, MNRAS, 363, 2
Kimm T. et al., 2009, MNRAS, 394, 1131
Larson R. B., 1974, MNRAS, 169, 229
Larson R. B., Tinsley B. M., Caldwell C. N., 1980, ApJ, 237, 692
Le Borgne D., Rocca-Volmerange B., Prugniel P., Lançon A., Fioc M., Soubiran C., 2004, A&A, 425, 881
Le Fèvre O. et al., 2004, A&A, 417, 839
Mac Low M.-M., Ferrara A., 1999, ApJ, 513, 142
Madau P., 1995, ApJ, 441, 18
Magorrian J. et al., 1998, AJ, 115, 2285
Mayer L., Kazantzidis S., Mastropietro C., Wadsley J., 2007, Nat, 445, 738
Mihos J. C., Hernquist L., 1996, ApJ, 464, 641
Moore B., Lake G., Katz N., 1998, ApJ, 495, 139
Moore B., Quilis V., Bower R., 2000, in Combes F., Mamon G. A., Charmandaris V., eds, ASP Conf. Ser. Vol. 197, Dynamics of Galaxies: from the Early Universe to the Present, Dynamical Effects on Galaxies in Clusters. Astron. Soc. Pac., San Francisco, p. 363
Morrissey P. et al., 2005, ApJ, 619, L7
Mouhcine M., Baldry I. K., Bamford S. P., 2007, MNRAS, 382, 801

Murray N., Quataert E., Thompson T. A., 2005, ApJ, 618, 569
Novikov D., Colombi S., Doré O., 2006, MNRAS, 366, 1201
Nuijten M. J. H. M., Simard L., Gwyn S., Röttgering H. J. A., 2005, ApJ, 626, L77
Ocvirk P., Pichon C., Teyssier R., 2008, MNRAS, 390, 1326
Ouchi M. et al., 2004, ApJ, 611, 660
Poggianti B. M., von der Linden A., 2006, ApJ, 642, 188
Pogosyan D., Bond J. R., Kofman L., Wadsley J., 1998, in Colombi S., Mellier Y., Raban B., eds, Wide Field Surveys in Cosmology Cosmic Web: Origin and Observables. Editions Frontières, Paris, p. 61
Postman M., Geller M. J., 1984, ApJ, 281, 95
Prunet S., Pichon C., Aubert D., Pogosyan D., Teyssier R., Gotloeber S., 2008, ApJS, 178, 179
Rasera Y., Teyssier R., 2006, A&A, 445, 1
Rimes C. E., 2009, MNRAS, 619, 0
Roediger E., 2009, Astron. Nachrichten, 330, 888
Salim S. et al., 2007, ApJS, 173, 267
Savaglio S. et al., 2005, ApJ, 635, 260
Schawinski K., Thomas D., Sarzi M., Maraston C., Kaviraj S., Joo S.-J., Yi S. K., Silk J., 2007, MNRAS, 382, 1415
Schawinski K. et al., 2006, Nat, 442, 888
Schaye J., Dalla Vecchia C., 2007, MNRAS, 383, 1159
Schlegel et al., 2007, BAAS, 38, 966
Scodeggio M., Vergani 2009, A&A, 501, 21
Scoville N. et al., 2007, ApJS, 172, 1
Silk J., Rees M. J., 1998, A&A, 331, L1
Sousbie T., Pichon C., Colombi S., Novikov D., Pogosyan D., 2008a, MNRAS, 383, 1655
Sousbie T., Colombi S., Pichon C., 2009, MNRAS, 393, 457
Sousbie T., Pichon C., Courtois H., Colombi S., Novikov D., 2008b, ApJ, 672, L1
Springel V., Di Matteo T., Hernquist L., 2005, MNRAS, 361, 776
Steidel C. C., Hamilton D., 1993, AJ, 105, 2017
Tanaka M., Goto T., Okamura S., Shimasaku K., Brinkmann J., 2004, AJ, 128, 2677
Tasca L. A. M. et al., 2009, A&A, 503, 379
Teyssier R., 2002, A&A, 385, 337
Toomre A., Toomre J., 1972, ApJ, 178, 623
Tweed D., Devriendt J., Blaizot J., Colombi S., Slyz A., 2009, A&A, 506, 647
van den Bosch F. C., Aquino D., Yang X., Mo H. J., Pasquali A., McIntosh D. H., Weinmann S. M., Kang X., 2008, MNRAS, 387, 79
van Dokkum P. G. et al., 2006, ApJ, 638, L59
Weinmann S. M., van den Bosch F. C., Yang X., Mo H. J., 2006, MNRAS, 366, 2
York D. G. et al., 2000, AJ, 120, 1579
Yoshikawa K., Yamasaki N. Y., Suto Y., Ohashi T., Mitsuda K., Tawara Y., Furuzawa A., 2003, PASJ, 55, 879

APPENDIX A: SELF-CONSISTENCY CHECKS

In this section, we present a few tests that were performed to check the presence of bias and the influence of the parameters of the skeleton and the MareNostrum simulation.

A1 Decorrelating galaxies with their environment

In order to check if our method induces artificial correlations of the galaxy properties with their environment, we shuffle the properties of the galaxies: for each galaxy, we change its colour to the colour of another randomly chosen galaxy, keeping its position unaffected. The results obtained on the shuffled sample, corresponding to Fig. 5, are presented in Fig. A1. As expected, the evolution of colour with the distance to filaments or nodes is totally erased.

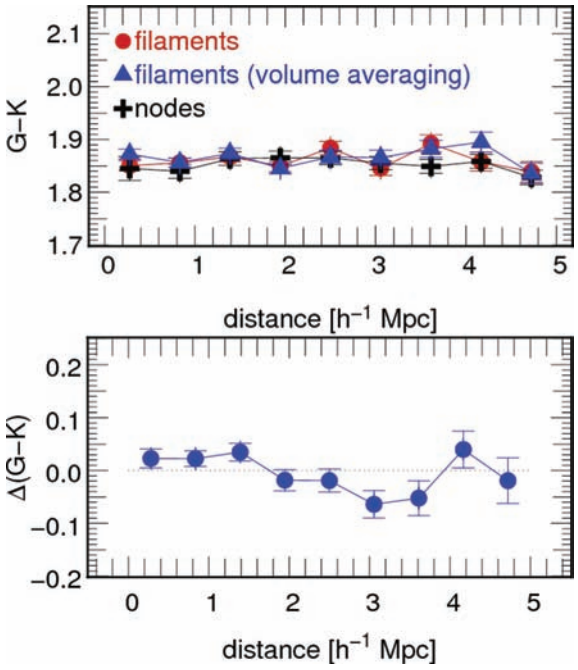

Figure A1. Same as Fig. 5 (top panel) and Fig. 7 (bottom panel) when galaxies properties are shuffled. As expected, the evolution is cancelled.

A2 The influence of smoothing

To compute the skeleton, the density field needs to be smoothed to ensure sufficient differentiability. The smoothing length is a free parameter, allowing one to probe different scales. All the previous results have been obtained with a Gaussian smoothing over $\sigma = 12$ pixels (with a 256^3 grid), which corresponds to 2 h^{-1} Mpc. Fig. A2 shows the results for a smoothing length of 8 and 16 pixels. Increasing the smoothing allows to select only the biggest features of the cosmic web. Thus, it changes the influence of the nodes in two different ways. First it increases the average colour near nodes, the reddest galaxies being located in the biggest clusters. Then it increases the influence scale of the nodes: galaxy properties can be influenced by the main clusters even at distances of several megaparsecs.

Nevertheless, the influence of the filaments is still vanishing when the influence of the clusters is correctly removed. Even the biggest filaments do not have a direct effect on the properties of galaxies.

A3 Spurious filaments

The fact that that some filaments of the skeleton could be spurious and would not correspond to any physical filaments could be responsible for the lack of dependence of spectroscopic properties with the distance to skeleton. This would lead to a dilution of the dependence, since the galaxies near spurious filaments would not be correctly taken into account. In order to check that the skeleton algorithm is not introducing such spurious filaments, we remove the less physical filaments. Considering whole filaments, i.e. a set of contiguous segments between two given nodes, ensure us that this procedure will not depend on the distance to nodes and will not introduce any bias. The selection criterion is based on the density of the underlying field, averaged over the filament. We choose a threshold such that up to 50 per cent of the skeleton is removed. The result of the pair comparison procedure is given in Fig. A3. It

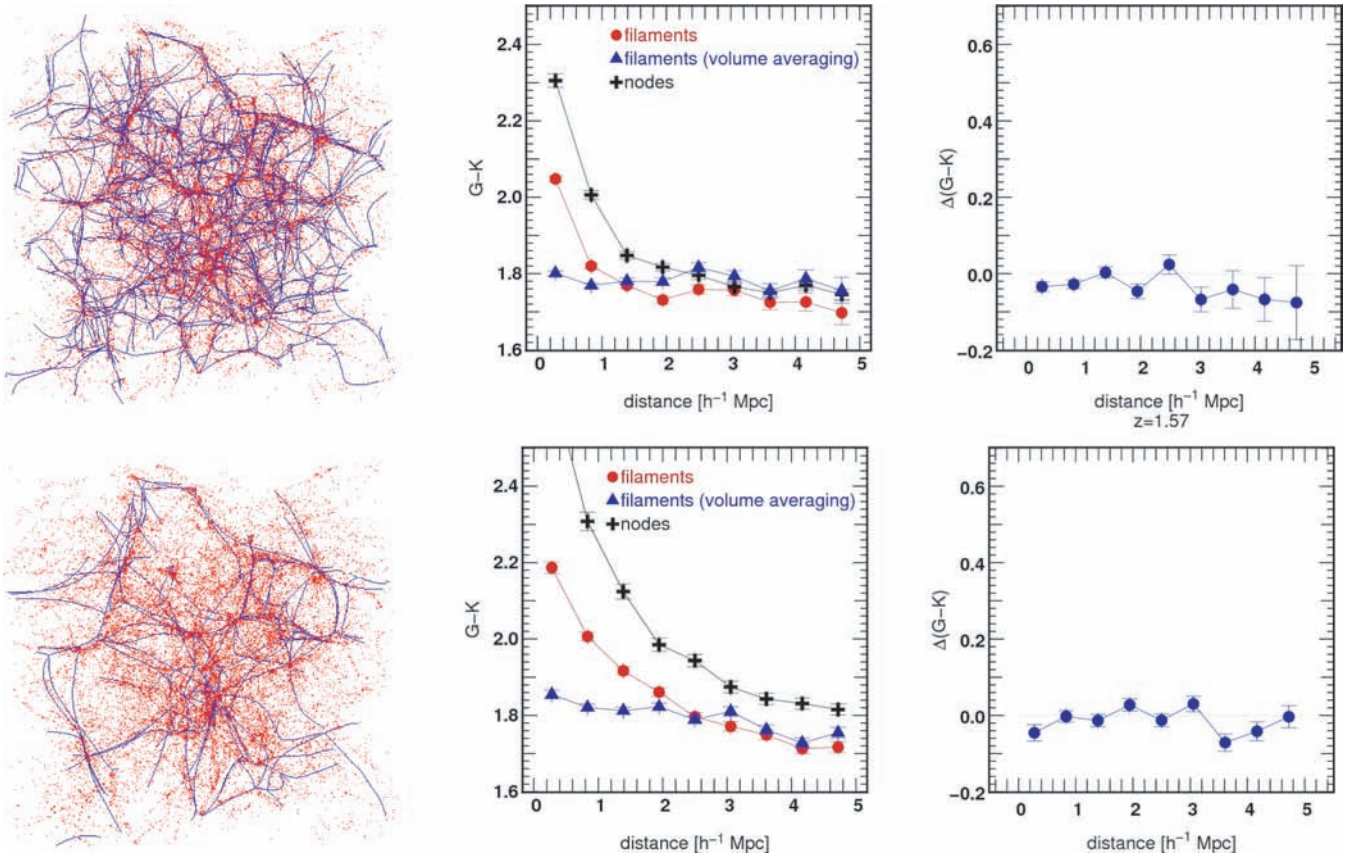

Figure A2. Left-hand panel: Galaxies (red) and skeleton (blue) for a smoothing length of 8 (top) and 16 (bottom) pixels. Increasing the smoothing length selects the main features of the cosmic web. Middle: same as Fig. 5 for a smoothing of 8 (top) and 16 (bottom) pixels. Right: same as Fig. 7 for a smoothing of 8 (top) and 16 (bottom) pixels.

shows that even when the less significant filaments produced by the skeleton algorithm are removed, the colour of the galaxies does not seem to depend on the distance to filaments. The result presented in the main text is therefore robust and cannot be explained as an artefact of the skeleton algorithm.

A4 A toy model for the observed colours

Deriving colours for objects in the simulation is a long and complex process, initiated from a model for the primordial density fluctuations and involving huge computing resources to grow the structures. As mentioned in Section 2.1, various approximations and recipes are required to obtain the end products of interest here, namely (virtual) galaxies.

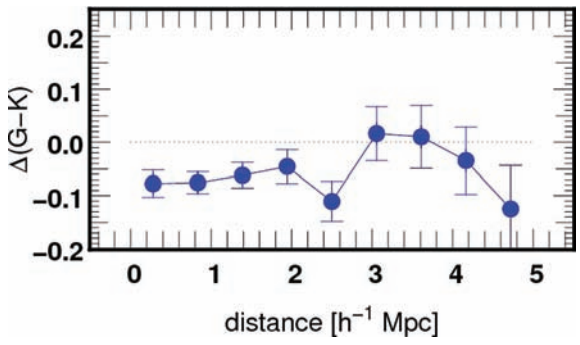

Figure A3. Same as Fig. 7 when the 50 per cent less dense filaments are removed. It shows that restraining to the more physical filaments does not change our findings.

To check that the colours presented here make sense with respect to what we know of galaxy colours today, we can either compare them to observations or to previous models. For simplicity, and to avoid potential biases inherent to observations done at various redshifts, we choose to test our results against a reasonably simple model of galaxy formation. Another reason to do so is that we did not include dust in the SED modelling of the simulation. A direct comparison with observations is therefore hazardous.

As a basis for this comparison, we use an idealized scenario with a smooth star formation history leading to the average colours of local late spiral Sd galaxies. Such a scenario is presented in Fioc & Rocca-Volmerange (1999) or Le Borgne et al. (2004). It involves the infall of primordial gas from a reservoir on to a potential well at a rate proportional to $\exp(-t/\tau)/\tau$ with $\tau = 6$ Gyr. As the accreted gas cools, stars begin to form with a Schmidt law, at a rate proportional to the gas density $\mathrm{SFR} = (14\ \mathrm{Gyr})^{-1}\rho_{\mathrm{gas}}$. Modelled with the code PEGASE.2, the metallicity of such a galaxy evolves consistently with the yields from SNe, and many physical properties are monitored, as well as predicted spectra and colours. These two timescales are the only parameters that were tuned to match the average colours of local star-forming galaxies with the hypothesis that the redshift of formation of the first stars is $z = 10$. In practice, choosing $z > 4$ produces an almost equally satisfying match for the observed colours.

This scenario, combined with others, is also successful in reproducing the galaxy counts in optical and near-infrared bands (Fioc

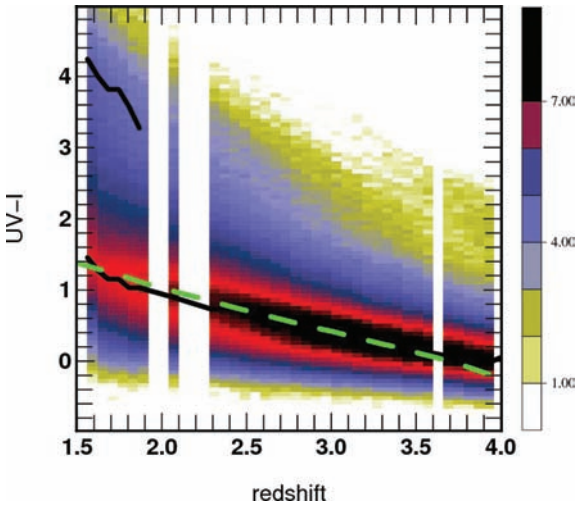

Figure A4. Evolution of the distribution of the rest-frame colour. Black lines: maximum and secondary maximum of the distribution. Green line: PEGASE model.

& Rocca-Volmerange 1999). Although such successes are appealing, they do not prove that the scenario is correct and it must be taken with caution. Still, we venture into the comparison of the MareNostrum simulated colours with the evolving colours derived from such an idealized scenario. We compare in Fig. A4 the evolving distribution of the UV-I rest-frame colour (which encompasses the 4000 Å break) for galaxies in the simulation with this so-called 'monolithic'' scenario. For consistency with the simulation, we do not include dust in the model for the Sd spiral. We find a remarkably good agreement between the colour peak of the blue sequence and the colour of the scenario at every redshift between $z = 1.6$ and 3, in a range where the refinement of the grid used for the simulation is comparable from one bound to the other. It suggests that the bulk of the galaxies might follow the path of the idealized scenario and end up in local late-type spirals. Such an agreement is comforting and suggests that the colours derived from the simulation are very reasonable in this redshift range. We must stress, however, that this comparison does not validate the monolithic scenario which was mainly tuned to reproduce $z = 0$ colours: the match of its colours with distant galaxies is much more difficult to check because of the difficulty to identify the progenitors of local spirals at higher redshift. And of course, this comparison cannot be used to argue that this cosmological simulation can be reduced to a monolithic collapse, which is contrary in nature to the hierarchical paradigm. Nevertheless, we might learn from this exercise that *on average*, the evolution of the population of blue galaxies in MareNostrum is driven by an *average* accretion rate following the natural law used above, and that *on average* the Schmidt law described above is representative of the global star formation activity. Still, the exact values of the time-scales used for our scenario should not be taken for granted: a significant degeneracy exists between them, not to mention the hypothesis made on the universality of the IMF.

The main outcome of this test is that the rest-frame colours that we produce seem coherent and are consistent, if we extrapolate them to $z = 0$ with the colours of local star-forming galaxies.

A5 MareNostrum simulation sanity check

Let us carry a couple of checks on the features of the MareNostrum simulation and its postprocessing using classical probes. Fig. A5

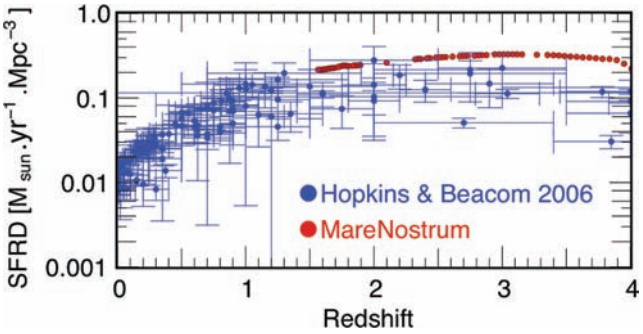

Figure A5. Comparison between the SFR in the MareNostrum simulation and in observed surveys (Hopkins & Beacom 2006). The virtual SFRD seems globally consistent, if somewhat high.

compares the SFR in the MareNostrum simulation and in the Hopkins & Beacom (2006) compilation. The virtual cosmic SFRD seems roughly consistent with the observed one (which is corrected for dust reddening), although on the high end. Fig. A6 compares the UV (1400 Å) rest-frame galaxy LF for galaxies measured in the MareNostrum simulation at redshift 4 uniformly extinguished with a Calzetti (2001) law of $E(B - V) = 0.22$, to that observed by Bouwens et al. (2007). Our simulated LFs at $z \sim 4$ are in good agreement with the available UV data (see Devriendt et al. 2009 for a more detailed comparison). The apparent discrepancy between the perfect agreement of the UV LFs and the slight overprediction of the SFRD can be explained by several factors: the $z = 4$ data points for the SFRD from Ouchi et al. (2004) are corrected with a dust extinction measured on individual objects, spanning a range of $E(B - V) \simeq 0.0$ to 0.4. Moreover, other uncertain factors are involved in the comparison, such as the correction for the IGM absorption or the model-dependent law to convert from UV luminosity to SFR.

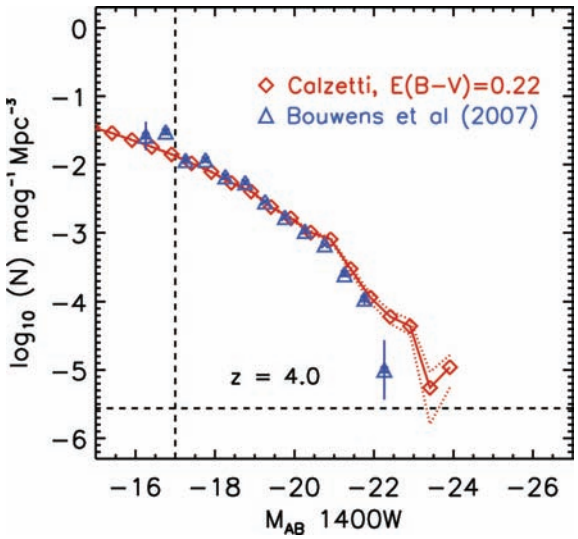

Figure A6. the UV (1400 Å) rest frame galaxy LF measured in the MareNostrum simulation at redshift 4. Red diamond LFs stand for galaxies uniformly extinguished with a Calzetti (2001) law. Blue triangles correspond to data gathered by Bouwens and collaborators (Bouwens et al. 2007). Vertical dashed lines indicate mass resolution, horizontal dashed lines volume resolution limits.

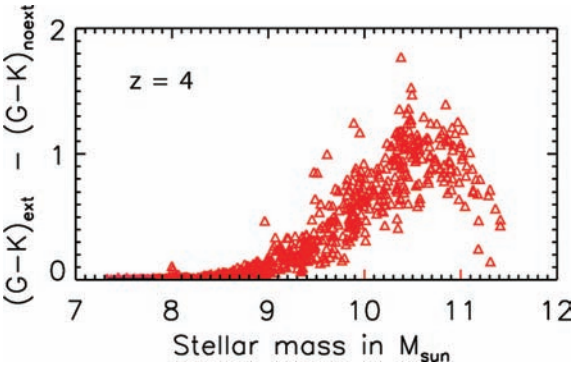

Figure A7. The effect of dust on $G - K$ colours as a function of stellar mass at redshift 4. Dust is modelled from the metallicity of a fair sub-sample of the underlying galaxy following the prescription of Devriendt et al. (2009). Note that the low-mass objects responsible for the bimodality described in this paper are not reddened.

A6 Tentative modelling of the effect of dust

Let us finally investigate the effect of dust on the $G - K$ colours computed in this paper. Following Devriendt et al. (2009), we compute the internal absorption of each galaxy using the metallicity of the gas within that galaxy as a proxy. Fig. A7 shows the difference in $G - K$ colours between the extinct and the non-extinct galaxies of the MareNostrum simulation at $z = 4$ as a function of galactic stellar mass. It reaches $\sim$1 mag at $\sim 10^{11}\,M_{\odot}$, but remains quite small for the low-mass satellites responsible for the observed bimodality.

Fig. A8 displays the same colour gradient as Fig. 5 (and Fig. 7) at redshift 4 for *reddened* $G - K$ colours; the corresponding unobscured colour gradients are shown as dashed lines. Taking into account the dust (i) produces a global shift of the colours and (ii) increases somewhat the colour gradient as a function of the distance to nodes, as massive (more obscured; see Fig. A7) galaxies are statistically more present at the nodes. Nevertheless the effect of dust on filaments remains much lower than the influence of nodes.

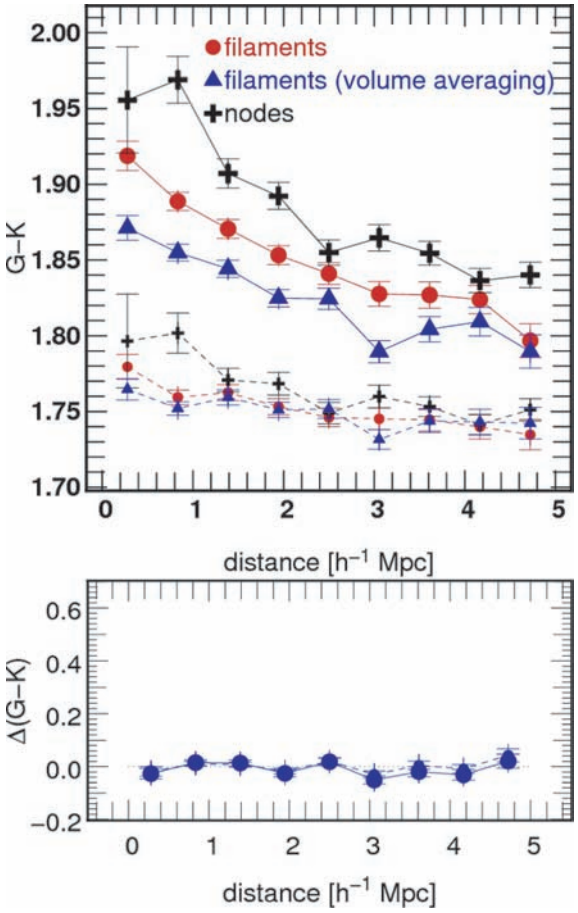

Figure A8. Same as Fig. 5 (top) and Fig. 7 (bottom) at higher redshift ($z = 4$) with (plain line) and without (dashed line) dust absorption. The net effect of dust is a global offset of the colours. The colour gradient for the nodes is slightly stronger with dust, which reflects the presence of massive dusty galaxies at the nodes, but does not modify our conclusions: filaments alone do not have a significant influence on the (dusty) colours of galaxies (bottom panel).

APPENDIX B: PHOTOMETRIC CATALOGUES

The data used in this study are made publicly available online: http://www.iap.fr/users/pichon/MareNostrum/catalogues. The catalogues contain the properties of the galaxies (position, colour, metallicity, age, SFR and stellar mass) and their environment (distance to skeleton and to nodes, corresponding densities) for redshifts 1.57, 1.8, 2.1, 2.51, 3.01, 3.53 and 3.95. The number of galaxies in each catalogue is, respectively, 97 563, 103 589, 111 184, 119 978, 124 642, 119 612 and 103 187. See Table B1 for a detailed list of the properties. The observed and the rest-frame colours are given by the magnitudes in the eight filters described in Table B2. Other filters could be implemented upon request. For the sake of simplicity, the skeleton is saved as a set of coordinates together with the mean dark matter density. The node catalogue follows the same prescription. Here, the catalogues are distributed as VOtables,[3] FITS and ASCII. These could be of use to anyone intending to compare this large-scale simulation to, e.g., observations at high redshifts. The skeletons are also available there for further investigation.

[3] http://www.ivoa.net/Documents/latest/VOT.html

APPENDIX C: SUBGRID PHYSICS

The simulation analysed in this paper relies on subgrid physics which we now briefly summarize.

C1 Star formation rate

Let us recall the method for implementing star formation in RAMSES as described in Rasera & Teyssier (2006). It is based on a phenomenological approach adopted in many, if not all, cosmological studies. It relies on observations of the scaling law between SFR and gas densities of local galaxies (Kennicutt 1998). Basically, one considers that star formation proceeds at a given time-scale, written here t_*, in regions where one or several physical criteria are fulfilled. We adopt a simple scheme to turn gas mass into star particles, adding a source term in the continuity equation

$$\left(\frac{\mathrm{D}\rho}{\mathrm{D}t}\right)_* = -\rho/t_*\,, \quad \text{if } \rho > \rho_0 = 0.1\,\mathrm{cm}^{-3},$$
$$\left(\frac{\mathrm{D}\rho}{\mathrm{D}t}\right)_* = 0\,, \qquad \text{otherwise,} \tag{C1}$$

Table B1. Content of the catalogues. The first and last galaxies of the catalogue at $z = 1.57$ are given as reference.

Name	Description	Unit	First	Last
xpos	X position	Mpc h^{-1}	0.201926	1.3122
ypos	Y position	Mpc h^{-1}	16.6967	45.9471
zpos	Z position	Mpc h^{-1}	47.9065	43.5113
redshift	Redshift	–	1.56506	1.56506
z_l	Luminosity-averaged stellar metallicity	dex	−1.69139	−2.97829
z_m	Mass-averaged stellar metallicity	dex	−1.78234	−3.03794
age_l	Luminosity-averaged stellar age	Myr	931.873	1429.32
age_m	Mass-averaged stellar age	Myr	1763.61	1640.19
FUV	Observed AB magnitude in the *FUV* band	mag	28.0128	47.3694
G	Observed AB magnitude in the *G* band	mag	20.9583	36.5068
R	Observed AB magnitude in the *R* band	mag	20.9726	35.7524
I	Observed AB magnitude in the *I* band	mag	20.8269	35.2413
z	Observed AB magnitude in the *z* band	mag	20.6424	34.8702
K	Observed AB magnitude in the *K* band	mag	19.3598	33.2805
IRAC3p6	Observed AB magnitude in the IRAC 3.6 μm band	mag	19.1845	33.252
IRAC8	Observed AB magnitude in the IRAC 8 μm band	mag	20.0335	34.2273
*FUV*_rest frame	Absolute (rest-frame) AB magnitude in the *FUV* band	mag	−25.3455	−9.4258
G_rest frame	Absolute AB magnitude in the *G* band	mag	−26.5264	−12.6057
R_rest frame	Absolute AB magnitude in the *R* band	mag	−23.829	−12.9374
I_rest frame	Absolute AB magnitude in the *I* band	mag	−26.9103	−13.0224
z_rest frame	Absolute AB magnitude in the *z* band	mag	−27.0163	−13.0619
K_rest frame	Absolute AB magnitude in the *K* band	mag	−36.8808	−12.6582
IRAC3p6_rest frame	Absolute AB magnitude in the IRAC 3.6 μm band	mag	−26.1501	−11.8306
IRAC8_rest frame	Absolute AB magnitude in the IRAC 8 μm band	mag	−24.7171	−10.2381
distance_skel	Distance to the skeleton	Mpc h^{-1}	0.371031	3.73985
distance_node	Distance to the nodes of the skeleton	Mpc h^{-1}	0.811432	5.69763
sfr	SFR	M$_\odot$ yr^{-1}	95.8817	0
stellar_mass	Total stellar mass	M$_\odot$	5.11478e+11	9.93592e+06

Table B2. Available filters.

Name	Reference	Mean wavelength (Å)
FUV Galex	Morrissey et al. (2005)	1520
G	Steidel & Hamilton (1993)	4810
R	Steidel & Hamilton (1993)	6980
I CFHT 12K	Le Fèvre et al. (2004)	8130
SDSS-*z*	Fukugita et al. (1996)	8960
Johnson K	Johnson et al. (1966)	21 950
Spitzer IRAC channel 1 IRAC-3.6 μm	Fazio (2004)	35 610
Spitzer IRAC channel 4 IRAC-8 μm	Fazio (2004)	79 580

where the star formation time-scale t_* is proportional to the local free-fall time

$$t_* = t_0 \left(\frac{\rho}{\rho_0}\right)^{-1/2}, \quad \text{with} \quad t_0 = 2\,\text{Gyr}. \tag{C2}$$

This choice of t_0 corresponds to the 5 per cent efficiency mentioned in the main text.

C2 Supernovae feedback

Following closely Dubois & Teyssier (2008), we define the mass vanished in the star formation process as

$$(\Delta m_g)_{\rm SF} = m_*(1 + \eta_{\rm SN} + \eta_W), \tag{C3}$$

where m_* is the final mass of the star particle, $\eta_{\rm SN}$ is the fraction of mass in SNe ejecta per solar mass of stars formed ($\eta_{\rm SN} = 0.1$ for the assumed Salpeter IMF) while η_W is the mass loading factor that determines the gas mass entrained by the SNe ejecta (which is set here to 1; see Dubois & Teyssier 2008). We assume that these debris are distributed according to a Sedov blast wave solution with a maximum speed given by

$$u_{\rm d} = \frac{u_{\rm SN}}{\sqrt{1 + \eta_W/\eta_{\rm SN}}}, \tag{C4}$$

where $u_{\rm SN}$ is the typical velocity corresponding to the kinetic energy released in one single SN explosion ($u_{\rm SN} \simeq 3200\,\text{km s}^{-1}$). The energy released to the gas by the debris is

$$E_{\rm d} = \eta_{\rm SN}\frac{m_*}{M_{\rm SN}}E_{\rm SN}, \tag{C5}$$

where $M_{\rm SN}$ and $E_{\rm SN}$ are respectively the typical progenitor mass and energy of an exploding Type II SN (i.e. $M_{\rm SN} = 10$ M$_\odot$ and $E_{\rm SN} = 10^{51}$ erg).

This paper has been typeset from a TEX/LATEX file prepared by the author.